Iteratively Reweighted Compressive Sensing Based Algorithm for Spectrum Cartography in Cognitive Radio Networks

B. A. Jayawickrama, E. Dutkiewicz
Macquarie University, Australia
Email: {beeshanga.abewardana, eryk.dutkiewicz}@mq.edu.au

I. Oppermann
CSIRO, Australia
Email: ian.oppermann@csiro.au

M. Mueck
Intel Mobile Communications, Germany
Email: markus.dominik.mueck@intel.com

***Abstract*—Spectrum cartography is the process of constructing a map showing Radio Frequency signal strength over a finite geographical area. In our previous work we formulated spectrum cartography as a compressive sensing problem and we illustrated how cartography can be used in the context of discovering spectrum holes in space that can be exploited locally in cognitive radio networks. This paper investigates the performance of compressive sensing based approach to cartography in a fading environment where realtime channel estimation is not feasible. To accommodate for lack of channel information we take an iterative approach. We extend the well-known iteratively reweighted ℓ_1 minimisation approach by exploiting spatial correlation between two points in space. We evaluate the performance in an urban environment where Rayleigh fading is prominent. Our numerical results show a significant improvement in the probability of accurately making a spectrum sensing decision, in comparison to the well-known weighted approach and the traditional compressive sensing based method.**

***Index Terms*—Cognitive Radio, Spectrum Cartography, Iteratively Reweighted Compressive Sensing, Rayleigh Fading.**

I. Introduction

Spectrum cartography can be envisioned as the process of plotting an attribute of the *Radio Frequency* (RF) environment over a finite geographical area. A common practice is to plot *Received Signal Strength* (RSS) in 2-dimensional space, considering a specific frequency of interest. We recognise the resulting plot in $\mathbb{R}^3$ as a *Radio Environment Map* (REM). Commercial software packages are widely used in the industry for spectrum cartography in network planning, maintenance and optimisation [1], [2]. Such commercial software packages can predict the coverage area and the capacity of a cellular base station assuming certain channel characteristics in the geographical area of interest. Although such applications are common, enabling *dynamic spectrum access* using spectrum cartography has not been well explored.

In a *cognitive radio network*, a mode of realising dynamic spectrum access, *Secondary Users* (SUs) utilise the spectrum without disrupting the communication of *Primary Users* (PUs). In traditional detect and avoid schemes, if a PU was discovered by a certain number of nodes sensing the spectrum, the whole network will avoid using that frequency. However, when the secondary network spans over a large area in comparison to the range of the PU network, SUs outside the range of the PU can safely use the bandwidth which enhances the spatial efficiency of spectral usage. Herein, spectrum cartography can be used as a powerful tool to determine the presence and the range of PU transmitters.

In [2], the authors propose to interpolate geolocalised *Received Signal Strength* (RSS) data in producing a REM. They use an interpolation technique called *Kriging Spatial Interpolation*, also used in many commercial network prediction software packages. In [3], the authors use the same interpolator and present an interference classification algorithm for dynamic spectrum access. In [4], the authors develop a testbed which constructs a REM assuming an inverse distance channel model. However, the work in [2]–[4] is only based on spatial interpolation techniques. The sparsity of PUs in multiple domains (time, frequency and space), which is common in many practical applications, is not exploited.

In our previous work [1], we formulated cartography as an ℓ_1 norm minimisation problem (i.e. a compressive sensing problem) exploiting the spatial sparsity of PUs. However, we considered only a distance based path loss channel model that was assumed to be known. In this paper, we extend our analysis into a fading environment. We assume the deterministic component of the channel related to path loss and large scale fading is known. However, the stochastic component arising from small scale fading is not known, also a posteriori estimation is not available. Under these circumstances the classic ℓ_1 norm minimisation approaches are less effective, hence we formulate a *weighted* ℓ_1 norm minimisation problem. The authors in [5] propose the well-known Iteratively Reweighted ℓ_1 norm (IRL1) algorithm for solving such problems. We extend IRL1 by exploiting the spatial correlation between two points in space. Our numerical results indicate that our approach is significantly more effective than classic compressive sensing as well as IRL1.

In Section II we present the system model. REM construction problem is formulated as a weighted ℓ_1 norm minimisation problem in Section III and our extension to IRL1 is illustrated in Section IV. Finally, numerical results are included in Section V.

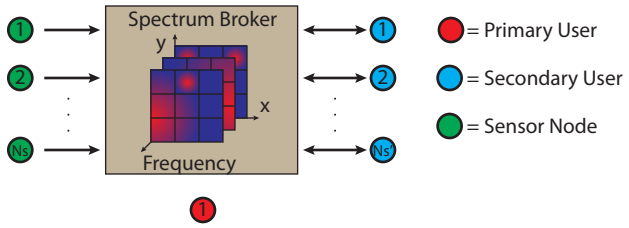

Fig. 1. System model: the Spectrum Broker collects RSS from sensor nodes and allocates available spectrum to SUs

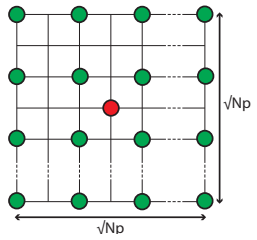

Fig. 2. The N_p point grid layout on which a PU is randomly located (dimension of $\sqrt{N_p} \times \sqrt{N_p}$ where $\sqrt{N_p} \in \mathbb{Z}^+$ is the number of points along one side of the square grid)

II. System Model

In our work, REM is defined as a map that shows the RSS value in $\mathbb{R}^2$ space for a certain frequency of interest. We assume the existence of a central entity named the *Spectrum Broker* that constructs a REM for each frequency of interest. System model is composed of N_s spectrum sensing nodes, N_s' SUs and 1 randomly located PU transmitter (system model is illustrated in Fig. 1).

Sensor nodes collect the RSS values and forward to the Spectrum Broker, along with their spatial coordinates. The Spectrum Broker constructs REMs for each frequency of interest indicating the corresponding geographical area where PU RSS is high. Generally, a PU receiver can decode a signal only if the SNR is higher than a minimum threshold. Therefore, the Spectrum Broker can determine the region where PU receivers are most likely to be present, assuming a reasonable threshold. This approach is similar to the interference temperature concept in IEEE 802.22 [6]. SUs are able to consult the Spectrum Broker to determine a frequency and the corresponding geographical region in which SUs can safely use that frequency without causing harmful interference to PU receivers. Further, we consider the interference between SUs and PUs only.

Additionally, we consider a $N_p (\gg N_s)$ point grid layout. Similar to [7], we consider that sensor nodes are uniformly distributed. Although we assume the presence of only one PU transmitter for simplicity, our work is still valid when multiple PUs are present as shown in our previous work [1]. To reduce the complexity of the problem in hand, we assume that sensor nodes and PUs are located on a grid as shown in Fig. 2. Although it can be criticised that assuming PUs are on a grid is less practical, clearly the system resolution can be increased by using a dense grid which minimises the error induced by this assumption. Even though we consider a dedicated static sensor network for simplicity in illustration, a sensor node could be a SU with spectrum sensing capability and the ability to determine its spatial coordinates using an external service such as the Global Positioning System (GPS).

We assume the existence of a common control channel between sensors, the Spectrum Broker and SUs to communicate RSS value and spectrum allocation information. Common spectrum sensing issues such as differentiating a PU signal from a SU signal at the sensing nodes can be overcome by assuming a quiet period or by using advanced schemes such as cyclostationary based detection. Such issues are beyond our scope, since this paper focuses only on the accuracy of spectrum sensing decisions in discrete space. In the rest of the paper, we limit our analysis to a single frequency REM, yet our work can be clearly replicated for multiple frequency bins of interest.

III. Problem Formulation

In this section we formulate REM construction as a weighted ℓ_1 norm minimisation problem. Let $\mathbf{P_s} \in \mathbb{R}^{N_s}$ be a column vector representing the RSS of the PU signals as measured by N_s sensors and $\mathbf{P_r} \in \mathbb{R}^{N_p}$ a column vector representing the RSS of PU signal at all N_p reference points in Fig. 2 (Note: $\mathbf{P_s} \subset \mathbf{P_r}$). Also, let $\mathbf{P_t} \in \mathbb{R}^{N_p}$ be a column vector in which the $1 \leq j^{\text{th}} \leq N_p$ element is defined as,

$$P_t(j) = \begin{cases} EIRP_j & \text{if a PU exists at the } j^{\text{th}} \text{ reference point} \\ 0 & \text{otherwise} \end{cases} \tag{1}$$

where $EIRP_j$ is the *Effective Isotropic Radiated Power* of the PU at j^{th} reference point. In our grid layout, shown in Fig. 2, the j^{th} reference point can be mapped to (row, column) coordinates as: $j \rightarrow (\lceil j/\sqrt{N_p} \rceil, j - \sqrt{N_p}(\lceil j/\sqrt{N_p} \rceil - 1)$. Assuming a *narrowband* channel in the presence of *Additive White Gaussian Noise* (AWGN), we write $\mathbf{P_r}$ as follows,

$$\mathbf{P_r} = \mathbf{\Psi P_t} + \boldsymbol{\eta} \tag{2}$$

where $\boldsymbol{\eta} \in \mathbb{R}^{N_p}$ is a column vector representing noise power at N_p reference points, $\mathbf{\Psi}$ is the $N_p \times N_p$ channel characteristic matrix defined as,

$$[\mathbf{\Psi}]_{ij} = F_{ij} G_{ij} L_{ij} : \forall 1 \leq i, j \leq N_p \tag{3}$$

where L_{ij} is the pathloss from point j to i, G_{ij} is a large scale shadow fading coefficient and F_{ij} models Rayleigh fading. $F_{ij} \forall 1 \leq i, j \leq N_p$ are independent and exponentially distributed random variables with unit mean. In a Rayleigh fading environment the signal envelope follows a Rayleigh distribution, but the received signal power follows an exponential distribution [8]. We assume that stochastic component of the channel F_{ij} is not known to the Spectrum Broker, however the deterministic component (i.e. $G_{ij} L_{ij}$) is assumed to be known. Hence, the expectation $E\left[[\mathbf{\Psi}]_{ij}\right] = G_{ij} L_{ij}$ is known.

The measured RSS values at sensors $\mathbf{P_s}$ can be written as,

$$\mathbf{P_s} = \mathbf{\Phi \Psi P_t} + \mathbf{\Phi} \boldsymbol{\eta} \tag{4}$$

where $\mathbf{\Phi}$ is the $N_s \times N_p$ geolocation matrix defined as follows $\forall 1 \leq j \leq N_p$ and $\forall 1 \leq k \leq N_s$,

$$[\mathbf{\Phi}]_{kj} = \begin{cases} 1 & \text{if } k^{\text{th}} \text{ sensor is at } j^{\text{th}} \text{ reference point} \\ 0 & \text{otherwise} \end{cases} \quad (5)$$

Since $\boldsymbol{\eta}$ is not zero mean we rearrange (4) as follows,

$$\mathbf{P_s} - \eta_{avg} = \mathbf{\Phi\Psi P_t} + \boldsymbol{\zeta} \quad (6)$$

where η_{avg} is the long term average AWGN power measured at the Spectrum Broker and $\boldsymbol{\zeta} \in \mathbb{R}^{N_s}$ is a column vector with error terms that provides for possible measurement errors at sensors.

We now have an underdetermined system of equations in (6). REM construction can be summarised as finding the expectation of $\mathbf{P_r}$. Our approach is to find *some* $\mathbf{P_t}$ by solving (6), then construct the REM as follows: $E[\mathbf{P_r}] = \mathbf{\Phi}E[\mathbf{\Psi}]\mathbf{P_t} + \eta_{avg}$. Since $\mathbf{P_t}$ is a sparse vector, we can formulate a classic ℓ_1 norm minimisation problem (i.e. a compressive sensing problem) as follows,

$$\arg\min_{\mathbf{P_t}} ||\mathbf{P_t}||_1 \text{ subject to } ||\mathbf{P_s} - \eta_{avg} - \mathbf{\Phi\Psi P_t}||_2 \leq \vartheta' \quad (7)$$

where $\|(\cdot)\|_p$ is the ℓ_p-norm of $(\cdot)$ $\forall p \in \mathbb{Z}^+$ and ϑ' is a constraint relaxation parameter providing for measurement errors. Due to the unknown stochastic element F_{ij} in $\mathbf{\Psi}$, the Spectrum Broker is unable to directly solve (7). Instead we solve,

$$\arg\min_{\mathbf{P_t}} ||\mathbf{P_t}||_1 \text{ subject to } ||\mathbf{P_s} - \eta_{avg} - \mathbf{\Phi}E[\mathbf{\Psi}]\mathbf{P_t}||_2 \leq \vartheta \quad (8)$$

However, the error introduced by solving (8) instead of (7) is substantial, as we illustrate further in Section V. To mitigate this harmful impact, we formulate a weighted problem as follows,

$$\arg\min_{\mathbf{P_t}} \sum_{i=1}^{N_p} \omega(i)|P_t(i)| \quad (9)$$

subject to:

$$||\mathbf{P_s} - \eta_{avg} - \mathbf{\Phi}E[\mathbf{\Psi}]\mathbf{P_t}||_2 \leq \vartheta$$

where $P_t(i)$ refers to the i^{th} element of $\mathbf{P_t}$ and $\boldsymbol{\omega}$ is a $N_p \times 1$ column vector of weights adjusted in each time iteration.

IV. Extended Iteratively Reweighted ℓ_1 Norm Minimisation Algorithm

In this section we present our extension to the well-known IRL1 algorithm. In [5] the authors investigate a weighted ℓ_1 norm minimisation problem, primarily in the context of image processing. They propose the following weight adjustment (IRL1),

$$\omega^{k+1}(i) = \frac{1}{|P_t^k(i)| + \gamma} \quad (10)$$

where $P_t^k(i)$ is the i^{th} element of k time sample of $\mathbf{P_t}$ and similarly $\omega^{k+1}(i)$ is the i^{th} element of $k+1$ time sample of the weight vector $\boldsymbol{\omega}$. The parameter $\gamma > 0$ provides stability and it also ensures zero elements in $\mathbf{P_t^k}$ do not strictly prohibit non zero estimates in $\mathbf{P_t^{k+1}}$ in the next step [5]. It is suggested that γ should be chosen as a value slightly smaller than the expected non zero values in $\mathbf{P_t}$ [5].

IRL1 is well known to outperform traditional (not weighted) ℓ_1 norm minimisation problems in general. However, in conventional ℓ_1 norm minimisation problems the orthogonal basis vectors are known a priori (i.e. ideal knowledge on channel estimates is available). In our REM construction application it is difficult to assume that realtime channel estimates are available, as it increases the overhead. In other words, we are unable to solve (7) directly, therefore we solve (9) by adjusting the weight ω as shown in Algorithm 1.

Algorithm 1 Extension to IRL1 Algorithm: k^{th} iteration

Require:

- $\boldsymbol{\omega^k}$ - $N_p \times 1$ column vector of weights calculated in the previous iteration. For $k = 1$ iteration choose the initial condition $\boldsymbol{\omega^1} = \mathbf{1}$
- P_{th} - minimum transmit power of the PU
- $0 < \alpha < 1$ - coefficient that determines the dependency of $\boldsymbol{\omega^{k+1}}$ on $\boldsymbol{\omega^k}$ i.e. the memory effect

1: **procedure** EXTENDED IRL1($\boldsymbol{\omega^k}, P_{th}, \alpha$)
2: Solve the following convex ℓ_1 minimisation problem

$$\arg\min_{\mathbf{P_t^k}} \sum_{i=1}^{N_p} \omega^k(i)|P_t^k(i)| \text{ subject to:}$$

$$||\mathbf{P_s^k} - \eta_{avg} - \mathbf{\Phi}E[\mathbf{\Psi}]\mathbf{P_t^k}||_2 \leq \vartheta$$

3: Calculate the weight vector for the next iteration $\boldsymbol{\omega^{k+1}}$ as follows
4: Initialise a temporary $N_p \times 1$ vector $\boldsymbol{\varpi}$ to hold weight adjustment considering spatial correlation between grid points
$\boldsymbol{\varpi} \leftarrow 1/\gamma$
5: **for all** $P_t^k(i) > P_{th}$ **do**
6: $\Lambda \leftarrow \{\text{Set of grid points spatially correlated with } i\}$
7: $\boldsymbol{\varpi}(\Lambda) \leftarrow \min\left(\boldsymbol{\varpi}(\Lambda), 1/(|P_t^k(i)| + \gamma)\right)$
8: **end for**
9: Calculate the weight vector for the next iteration $\boldsymbol{\omega^{k+1}} = \alpha\boldsymbol{\omega^k} + (1-\alpha)\boldsymbol{\varpi}$
10: **end procedure**

In Line 2, we use the $\boldsymbol{\omega^k}$ (calculated in the previous iteration) find a solution for $\mathbf{P_t^k}$, similar to IRL1. However, our algorithm is significantly different from IRL1 due to the weight computation in Line 3-9. Due to noisy measurements and unknown stochastic element in $\mathbf{\Psi}$, convex optimisation results in a large number of non zero (near zero however) entries in $\mathbf{P_t^k}$. A non zero entry in $\mathbf{P_t^k}$ implies the presence of a PU transmitter as per the definition in 1). Hence, such values that are unreasonably small for the transmit power of a potential PU need to be removed, for this filtering we use a minimum threshold in Line 5. In Line 6 we find the set of grid points that are neighbouring to point i and adjust the

corresponding weights (a neighbourhood can be discovered as we illustrated in [1]). Hence in Algorithm 1, a non zero entry at i has an influence on the weights corresponding to a set of neighbouring points, whereas in IRL1 such an entry would affect only one entry in $\boldsymbol{\omega}$. Additionally, in Line 9 we take the weighted average of $\boldsymbol{\omega^k}$ and $\boldsymbol{\varpi}$. Therefore, $\boldsymbol{\omega^{k+1}}$ has a strong dependency on $\boldsymbol{\omega}$ from previous iterations. This helps in mitigating the impact of the incompleteness of compressive sensing dictionary.

V. Simulation and Analysis

In this section we present our simulation setup and the results showing the effectiveness of our algorithm. We construct a REM using classic ℓ_1 norm minimisation (compressive sensing) and also using weighted ℓ_1 norm minimisation where the weight was adjusted as per IRL1 in [5] and the proposed algorithm in this paper. For solving convex problems we use the well-known SeDuMi solver [9].

In our setup, we assume a 11×11 point grid and sensor nodes at every other grid point as shown in Fig. 2 (i.e. $N_p = 121$ and $N_s = 36$). We use the pathloss and large scale fading parameters found in the WINNER+ UMi channel model [10], which is the TV White Space frequency extension of the 3GPP channel model. A PU is located at a randomly selected grid point and we run an experiment for 1000 iterations.

Since we are using a discrete space model, the performance evaluation criteria is the proportion of grid points where *False Alarm* (FA) and *Missed Detection* (MD) occur. FA and MD at point i are defined as follows,

$$\mathbf{H_0(i)}: \quad \text{RSS at point } i < P_{th} \quad \text{(i.e. } \exists \text{ a spectrum hole)}$$
$$\mathbf{H_1(i)}: \quad \text{RSS at point } i \geq P_{th} \quad \text{(i.e. } \nexists \text{ a spectrum hole)}$$

$$N_{fa} = \quad \text{Number of points where } \mathrm{H_1|H_0} \tag{11}$$
$$N_{md} = \quad \text{Number of points where } \mathrm{H_0|H_1} \tag{12}$$

Therefore the proportion of area with FA and MD are the ratios N_{fa}/N_p and N_{md}/N_p respectively, the evaluation criteria. The IEEE 802.22 standard does not provide a default value for the decision threshold P_{th}, a range is stated however as $-120 \leq P_{th} \leq -10$ dBm [6]. The threshold is said to be subject to the type of application. Therefore we select $P_{th} = -70$ dBm which falls well within the range.

A. Detecting the PU active region

In Fig. 3 we show the contour plot of RSS at P_{th}. The *Actual RSS* plot shows a heat map of RSS resulted by a PU. The red area is where the PU is present, the RSS is high. As the colour turns into blue the RSS is lower. The other three plots in Fig. 3 show the contour at the selected P_{th}. We notice that the contour resulted by our iteratively reweighted ℓ_1 approach closely follows the expected. The IRL1 approach and the traditional compressive sensing approaches result in a large FA area (the white area surrounded by red contours), in comparison to the FA area of our approach. However, all three methods seem similar in terms of the MD area, except

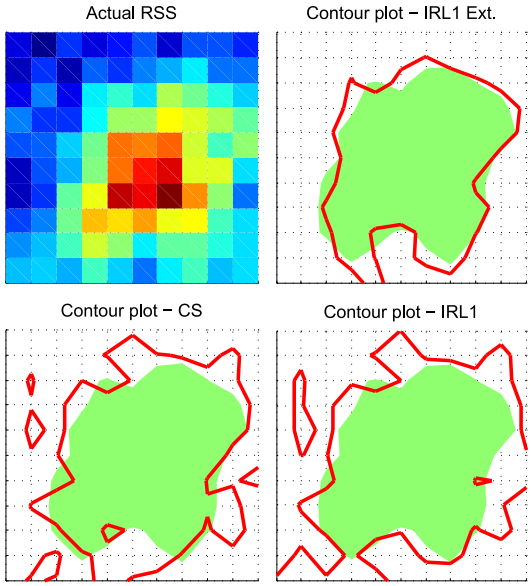

Fig. 3. The expected REM and contour plots from each method. The green area is where $\mathrm{H_1|H_1}$ occurs (i.e. no spectrum hole, a PU is present). The white area is where $\mathrm{H_0|H_0}$ occurs. The red line shows the boundary of PU active area obtained from each method.

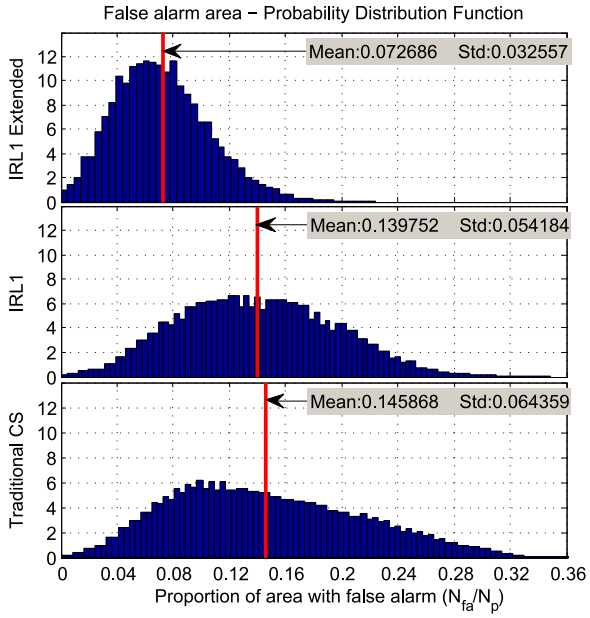

Fig. 4. Empirical Probability Distribution Function of the false alarm area. Mean of the distribution is marked with a red line

for the small island shapes in the green area of compressive sensing and IRL1 plots in Fig. 3. The rest of Section V further analyses the FA area and MD area.

B. False alarm area

The empirical Probability Distribution Function (PDF) of the ratio N_{fa}/N_p is shown in Fig. 4. Plots are normalised such that the integral of the bar graph results in 1, a fundamental requirement in a PDF. The ratio N_{fa}/N_p corresponds to the

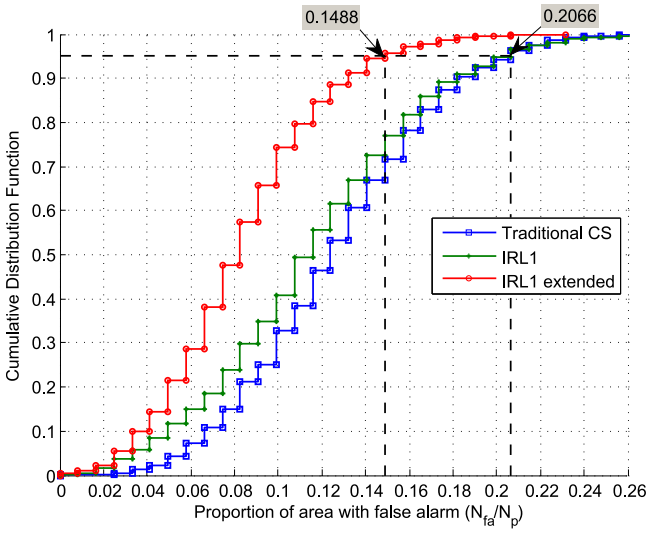

Fig. 5. Empirical Cumulative Distribution Function of the false alarm area. The 95% probability level is marked with broken black lines

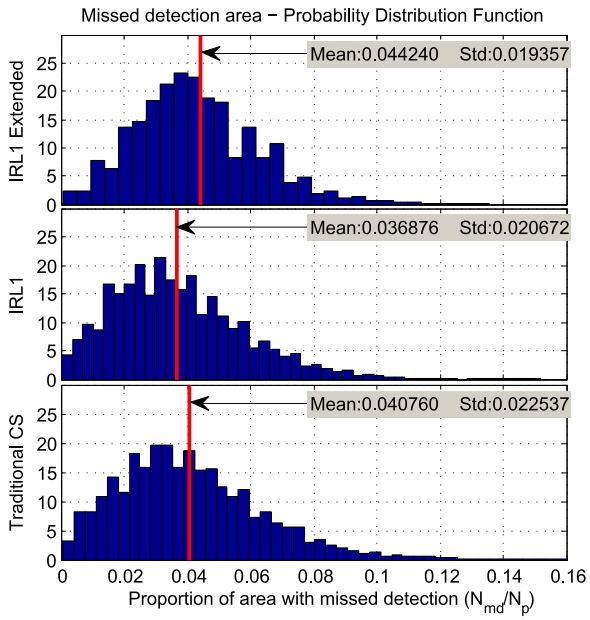

Fig. 6. Empirical Probability Distribution Function of the missed detection area. Mean of the distribution is marked with a red line. Note: scales are different from Fig. 4 (especially the x scale)

percentage of the area that encountered a FA. The Fig. 4 clearly shows that our algorithm results in a tall and narrow distribution. The mean and standard deviation for each distribution are also shown in Fig. 4. On average our approach results in only 7.27% of FA area, this is the percentage of area with undiscovered spectrum opportunities. In comparison to other approaches, the mean has been improved by at least 48% ($\approx (13.98-7.27)/13.98$). Further, the standard deviation has been dropped down to 3.26% of space, which is at least a 40% ($\approx (5.42-3.26)/5.42$) improvement.

For further analysis we plot the empirical Cumulative Distribution Function (CDF) of the ratio N_{fa}/N_p in Fig. 5. IRL1 marginally outperforms the traditional approach, however our algorithm results in significantly less FA area in comparison to both other approaches. Extended IRL1 ensures with 95% probability that FA occurs in less than 14.88% of the space. Both other methods can only guarantee that FA area is less than 20.66%, which indicates a significant improvement.

Our algorithm is able to closely follow the contours of high PU activity area, the green area shown in Fig. 3. Both other methods are not as effective as our approach in following the contours, which helps to improve the FA area in Fig. 4 and Fig. 5.

C. Missed detection area

In Fig. 6 we show the empirical probability distribution function for MD area (i.e. N_{md}/N_p). In our proposed method, the standard deviation has been improved. The mean however appears to have worsened marginally. By careful observation we discover that mean values of all three distributions fall well within 0.73% ($= 0.0442 - 0.0369$), and the standard deviations fall within 0.31% ($= 0.0225 - 0.0194$). Therefore we conclude that the difference is not significant enough for statistical inference.

As shown in Fig. 3, the IRL1 and conventional compressive sensing approaches tend to result in a larger area surrounded by red contours in comparison to the green area. In other words, the FA area is prominent in those two methods. However, the MD area, which is already marginal, is essentially similar in all three methods. This explains the result in Fig. 6, all three methods lead to similar MD areas, although the FA area was improved significantly.

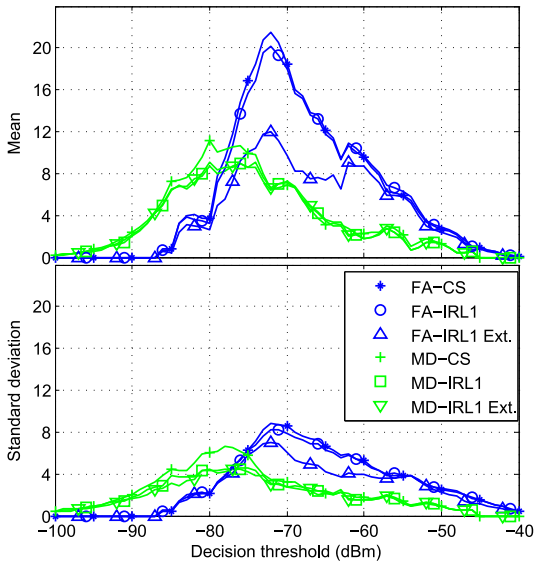

Fig. 7. Impact of the decision threshold. Mean and standard deviation values for a range of thresholds is shown for all three methods under evaluation

D. Impact of the decision threshold

In previous experiments we selected the detection threshold $P_{th} = -70$ dBm. To determine the impact of this threshold on the results, we vary it from -100 dBm to -40 dBm. We

calculate the mean and standard deviation of the FA area (N_{fa}/N_p) and MD area (N_{md}/N_p) in each method for a set of random locations of a PU. The results are shown in Fig. 7. Extended IRL1 appear to result in lower FA mean and standard deviation in the threshold range $[-80, -60]$ dBm. Although our approach outperforms MD of conventional compressive sensing in the range $[-80, -75]$ dBm, we prudently conclude that the difference is not substantial for statistical inference. Therefore we determine that our algorithm outperforms both other methods discussed in this paper in terms of FA area, over a pragmatic range of the detection threshold.

VI. Conclusion

In our previous work [1] we proposed how a compressive sensing (ℓ_1 minimisation) problem can be formulated for spectrum cartography. In this paper we extended our previous work to a Rayleigh fading environment. We investigated the scenario where realtime channel estimation is not feasible, as such estimation imposes a large overhead. The main challenge in applying compressive sensing techniques in this scenario is the presence of an unknown stochastic element in the dictionary, due to unavailability of realtime channel estimation. We were able to overcome this by formulating a *weighted* ℓ_1 norm minimisation problem. We proposed an extension to the well known IRL1 algorithm in [5] that solves weighted ℓ_1 norm problems. Numerical results indicates that our algorithm is able to closely follow the border of a PU active area. Although the improvement in Missed Detection area was concluded not substantial enough for statistical inference, our algorithm results in a significantly smaller False Alarm area in comparison to the traditional compressive sensing technique and IRL1. Improvement in False Alarm area is approximately 50% of mean, 40% of standard deviation and 30% of 0.95 probability cut off.

References

[1] B. A. Jayawickrama, E. Dutkiewicz, I. Oppermann, G. Fang, and J. Ding, "Improved performance of spectrum cartography based on compressive sensing in cognitive radio networks," in *IEEE ICC 2013 - Wireless Communications Symposium (ICC'13 WCS)*, Budapest, Hungary, Jun. 2013.

[2] A. Alaya-Feki, S. Ben Jemaa, B. Sayrac, P. Houze, and E. Moulines, "Informed spectrum usage in cognitive radio networks: Interference cartography," in *Personal, Indoor and Mobile Radio Communications, 2008. PIMRC 2008. IEEE 19th International Symposium on*, sept. 2008, pp. 1 –5.

[3] R. Mahapatra and E. Strinati, "Interference-aware dynamic spectrum access in cognitive radio network," in *Personal Indoor and Mobile Radio Communications (PIMRC), 2011 IEEE 22nd International Symposium on*, sept. 2011, pp. 396 –400.

[4] D. Denkovski, V. Rakovic, M. Pavloski, K. Chomu, V. Atanasovski, and L. Gavrilovska, "Integration of heterogeneous spectrum sensing devices towards accurate rem construction," in *Wireless Communications and Networking Conference (WCNC), 2012 IEEE*, april 2012, pp. 798 –802.

[5] E. Candès, M. Wakin, and S. Boyd, "Enhancing sparsity by reweighted ℓ_1 minimization," *Journal of Fourier Analysis and Applications*, vol. 14, no. 5-6, pp. 877–905, 2008. [Online]. Available: http://dx.doi.org/10.1007/s00041-008-9045-x

[6] "IEEE Standard for Information technology– Local and metropolitan area networks– Specific requirements– Part 22: Cognitive Wireless RAN Medium Access Control (MAC) and Physical Layer (PHY) specifications: Policies and procedures for operation in the TV Bands," *IEEE Std 802.22-2011*, pp. 1–680, 2011.

[7] B. A. Jayawickrama, E. Dutkiewicz, I. Oppermann, M. D. Mueck, and G. Fang, "Downlink power allocation algorithm for licence-exempt LTE systems using kriging and compressive sensing based spectrum cartography," in *Globecom 2013 - Wireless Communications Symposium (GC13 WC)*, Atlanta, USA, Dec. 2013.

[8] S. Kandukuri and S. Boyd, "Optimal power control in interference-limited fading wireless channels with outage-probability specifications," *Wireless Communications, IEEE Transactions on*, vol. 1, no. 1, pp. 46–55, 2002.

[9] M. Grant and S. Boyd, "CVX: Matlab software for disciplined convex programming, version 1.22," Feb. 2012. [Online]. Available: http://cvxr.com/cvx

[10] J. Meinila, P. Kyosti, L. Hentila, T. Jamsa, E. Suikkanen, E. Kunnari, and M. Narandzia, "D5.3: WINNER+ Final Channel Models," Celtic Telecommunication Solutions, Tech. Rep., June 2010.